Facile Synthesis of Hollow CuO/MWCNT Composites by Infiltration-Reduction-Oxidation Method as High Performance Lithium-ion Battery Anodes

Gang Zheng, Zhiang Li*, Jinhua Lu, Jinhua Zhang, Long Chen[†], and Maoping Yang[†]

Gotion High-Tech Co. Ltd. No. 599, Daihe Road, Xinzhan District, Hefei, Anhui, China

ABSTRACT

Hollow copper oxide/multi-walled carbon nanotubes (CuO/MWCNT) composites were fabricated via an optimized infiltration-reduction-oxidation method, which is more facile and easy to control. The crystalline structure and morphology were characterized by X-ray diffraction (XRD), and transmission electron microscopy (TEM). The as-prepared CuO/MWCNT composites deliver an initial capacity of 612.3 mAh·g^{-1} and with 80% capacity retention (488.2 mAh·g^{-1}) after 100 cycles at a current rate of 0.2 A·g^{-1}. The enhanced electrochemical performance is ascribed to the better electrical conductivity of MWCNT, the hollow structure of CuO particles, and the flexible structure of the CuO/MWCNT composites.

1. Introduction

The ever-growing demand for energy storage system in electric vehicles (EVs), hybrid electrical vehicles (HEVs) and portable electronic devices such as mobile phones, tablets and laptops has accelerated the consumption of lithium ion batteries (LIBs) [1-2]. As the state-of-the-art anode material for most of the commercial lithium ion batteries currently, graphite has several advantages such as low prices, abundant, readily available and non-toxic [3-4]. But the low capacity (theoretical capacity is 372 mAh·g^{-1}) hinder its application in extreme high energy density LIBs. Recently, transition metal oxides have attracted much attention for the next generation promising anode materials due to the remarkably high specific capacities [5-10]. Copper oxide (CuO), as one of these transition metal oxides family, its high theoretical capacity (670 mAh·g^{-1}), nontoxic, easily produced and affordable price [11] suggest it a better commercial application in next-generation LIBs.

As known to all, the high theoretical capacity of CuO bases on the conversion reactions CuO + 2Li$^+$ + 2e$^-$ ↔ Li$_2$O + Cu. During the transition, the excessive volume change can induce particles pulverization, leading to a rapid deterioration of the reversible capacity [12]. In addition, its poor conductivity leads to the poor rate performance [13]. Nowadays, some methods like preparing nano-sized materials, coating or doping carbon materials to form composite materials, have been put forward to overcome these problems [14-17]. Morphology control is also an effective method to improve the performance of the material. Specific morphologies of CuO particles such as hollow sphere, nanotube, nanosheet, porous-like have been synthesized in recent year [18-21]. But the synthetic processes of these CuO particles with different morphologies are considerably complex, difficult to control and scale up. So the synthetic processes need to be further improved before adopted in commercial production.

In this work, we adopted a new method (infiltration-reduction-oxidation method) to synthesize the hollow CuO combined with multi-walled carbon nanotube (MWCNT). The synthesize processes is more facile and easy to control. The electrochemical

---

performances of CuO/MWCNT composites were studied. The results show that combining the hollow CuO and MWCNT can not only enhance the rate capacity of CuO particles, but also buffer the large volume change during the lithium insertion/extraction process. The CuO/MWCNT composites have much better rate cyclability and cycle performance.

2. Experiments

The MWCNTs (99.2%) are purchased from Sanshun Zhongke New Materials Co., Shenzhen, China. The length, diameter and specific surface of MWCNT are 5-12 μm, 30-50 nm and 85-110 $m^2 \cdot g^{-1}$, respectively. All other reagents used in the present study are analytical grade and purchased from Sinopharm Chemical Reagent Co., Shanghai, China.

2.1 The synthesis of CuO/MWCNT composites
The CuO/MWCNT composites were synthesized by an optimized infiltration-reduction-oxidation method: 107 mg $CuCl_2 \cdot 2H_2O$ and 60 mg MWCNTs were added into 15 ml deionized water. After 15 min ultrasonic dispersion, the suspension were heated to 60^oC under alternately magnetic stirring and ultrasonic dispersion until they became slurry like. Then the slurry were put into a vacuum oven to evaporate the distilled water at 40^oC for 12 h. Subsequently, the dried sample were grinded to powder. Then the powder was put into a tube furnace and heated to 350^oC for 2 hours at a rate of $10^oC \cdot min^{-1}$ with an Ar/H_2 atmosphere, followed by a treatment at 350^oC for 10 hours in air condition. At last, the CuO/MWCNT composites were obtained. For comparison, pure CuO particles were prepared by directly evaporating the $CuCl_2 \cdot 2H_2O$ solution and experienced a parallel calcination process.

2.2 Material characterization
Crystal structure of the products was characterized by X-ray diffraction (XRD, Rigaku SmartLab) with Cu Kα radiation. Thermogravimetric (TG) analysis of the CuO/MWCNT composites was processed by thermal analysis apparatus (TG, STA449C, German Netzsch). The morphology was examined by transmission electron microscope (TEM, JEM-2100, JEOL).

2.3 Electrochemical measurements
The electrochemical performance was evaluated using CR2032 coin cells. The working electrode was prepared by casting slurries, consisting of the as-prepared powder, Super P carbon black, and polyvinylidene fluoride (PVDF) in a weight ratio of 8:1:1 and with N-methyl-2-pyrrolidine (NMP) as solvent, on a copper foil. Subsequently, the electrode was dried at 80^oC for 12 h in the vacuum oven. The electrode density of the CuO/MWCNT is 1.6 $g \cdot m^{-2}$. The amount of active materials (CuO) was controlled as the same either in the CuO/MWCNT electrode or in the CuO electrode. The separator was a polypropylene membrane (ND14, Shanghai Energy New Materials Technology Co., China). Lithium metal was used as counter and reference electrode. The electrolyte was 1 M $LiPF_6$ in a mixture of ethylene carbonate (EC) and diethyl carbonate (DEC) (1:1 volume). Galvanostatic charge-discharge experiment was conducted using NEWARE Cell test system in the voltage range of 0.05-3.0 V (vs. Li^+/Li). Cyclic voltammetry was performed on a CHI660D electrochemical workstation (Shanghai Chenhua Co.) at a scan rate of 0.1 $mV \cdot s^{-1}$. The Electrochemical Impedance Spectroscopy (EIS) were collected by Autolab electrochemical workstation.

3. Results and Discussion

3.1 Crystal structure and morphology of the CuO/MWCNT composites
The phase composition of CuO and CuO/MWCNT composites were examined by XRD, as shown in Fig. 1. The diffraction peaks of pure CuO sample are consistent with the standard diffraction pattern of CuO (JCPDS 98-008-7125). The diffraction peaks at 32.61, 35.62, 38.78, 48.99, 53.62, 58.22, 61.65, 66.34, 68.16, 72.61 and 75.21 degree can be indexed to (110), (11$\bar{1}$), (111), (20$\bar{2}$), (020), (202), (11$\bar{3}$), (31$\bar{1}$), (220), (311) and (22$\bar{2}$) crystal planes of CuO. After combining with MWCNT, there is a diffraction peak near 26.08 degree that corresponds to the (002) standard diffraction pattern of Carbon (JCPDS-98-005-2230). The broadened and weaker peak in the XRD spectrum indicates a nano-scale crystal size of CuO particles [22]. No peaks related to any other impurities were detected in the XRD pattern. To measure the content of MWCNTs in the CuO/MWCNT composites, a TG test in air atmosphere at a heating rate of $10^oC \cdot min^{-1}$ was conducted, as shown in Fig. 2. At the beginning of 30 to 200^oC, about 0.1% weight
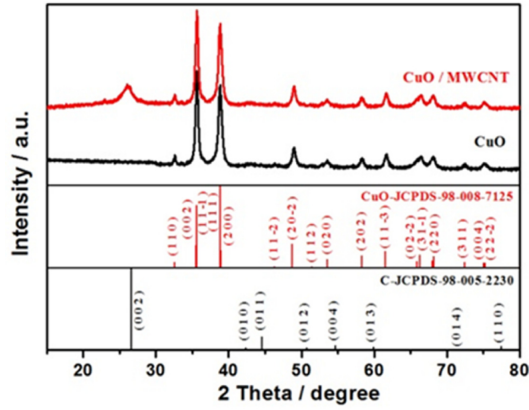
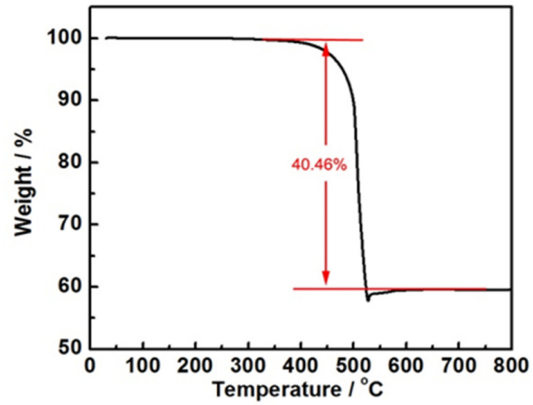**Fig. 1.** XRD patterns of pure CuO and the CuO/MWCNT composites.

Fig. 2. TG curve of the CuO/MWCNT composites in air atmosphere.
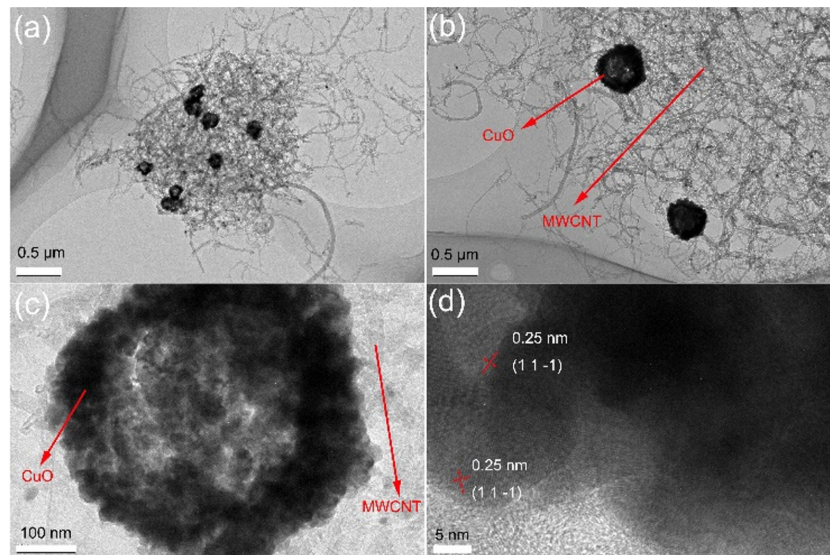

Fig. 3. TEM and HRTEM micrographs of CuO/MWCNT composites.

loss was detected. This can be attributed to evaporation of the adsorbed water in the composites. A large weight loss occurs from 320 to 528°C, corresponding to the oxidation decomposition of carbon nanotubes and the redox reaction between carbon and copper oxide carbon [23]. When the temperature was higher than 528°C, the weight increment was attributed to the Cu_2O oxidized to CuO. From 320 to 700°C, 40.46% weight loss was detected. Therefore, the mass percentage of CuO in the CuO/MWCNT composites is about 59.54%.

The TEM and the high resolution TEM (HRTEM) were performed to confirm the morphology of CuO/MWCNT composites. As shown in in Fig. 3 (a), the dark black ball like particles with a diameter of 300-500 nm refer to the CuO particles. The light gray noodles like agglomeration are the MWCNTs. It also indicates that CuO particles have deposited on the surface of MWCNTs. Fig. 3(c) is the enlarge TEM image of sample. During the synthesis of CuO/MWCNT composites, the CuO first reduced by hydrogen and then oxidized to CuO. Due to the
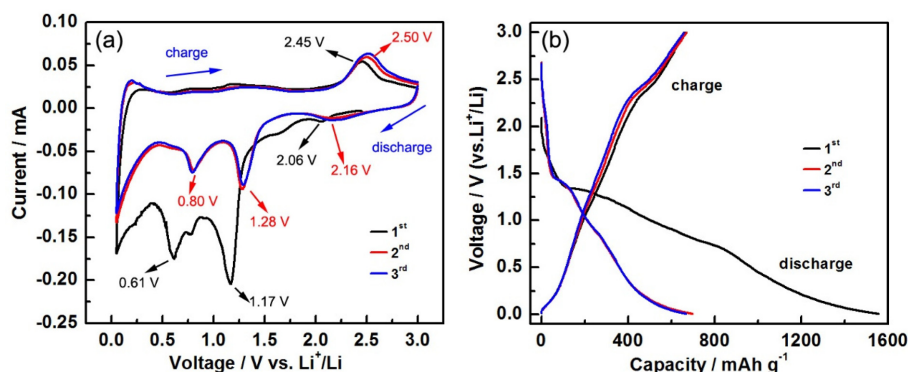
Fig. 4. (a) The first three CV curves of CuO/MWCNT composites in the potential range of 0.01–3.0 V at a scan rate of 0.1 mV·s^{-1}; (b) Charge–discharge voltage profiles of the CuO/MWCNT composites at the rate of 0.2 A·g^{-1};

Kirkendall Effect [24], the hollow structure of CuO particles are successfully synthesized. The hollow structure of CuO particles can be clearly observed. Furthermore, MWCNTs with a diameter of 30-50 nm are binding to the CuO particles, which indicates a well combination between them. Fig. 3(d) shows the HRTEM images of CuO particles. The lattice fringe with an interplanar distance of 0.25 nm refers to the $(11\bar{1})$ plane of CuO crystals. The XRD results and TEM images suggest that CuO/MWCNT composites with high quality are obtained.

3.2 Electrochemical performance of the CuO/ MWCNT composites

The cyclic voltammogram (CV) curves and the galvanostatic charge–discharge curves of the CuO/ MWCNT composites are shown in Fig. 4. In the first discharge process of the CuO/MWCNT electrode, as shown in the Fig. 4(a), three cathodic peaks locate at 2.06, 1.17, and 0.61 V (vs. Li$^+$/Li) can be detected. The weaker broad peak ~2.06 V corresponds to the solid solution formation of Li$_x$CuO [25]. The prominent peak at 1.17 V could be ascribed to the formation of intermediate Cu$_2$O phase (2CuO + 2Li$^+$ + 2e$^-$ → Li$_2$O + Cu$_2$O) and its association with structural destruction as well [26]. Another implicit reduction peak at 0.61 V corresponds to further reduction of Cu$_2$O to purity Cu (Cu$_2$O + 2Li$^+$ + 2e$^-$ → Li$_2$O + 2Cu) [26]. During charge process, the peak at 2.45 V corresponds to the oxidation of Cu into Cu$_2$O and subsequently converted into CuO as well (Cu + Li$_2$O → 2Li$^+$ + CuO +2e$^-$) [25]. In the second charge and discharge processes, three cathodic peak potentials
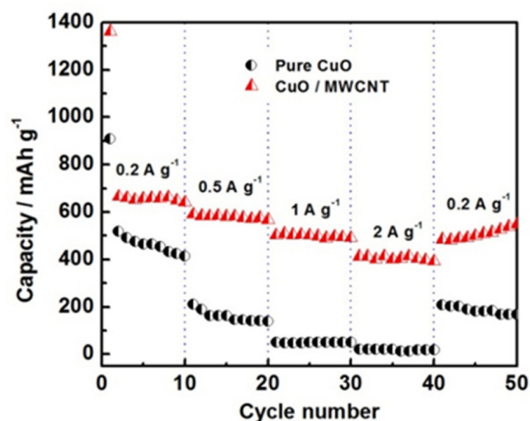

Fig. 5. Rate cyclability of pure CuO and CuO/MWCNT composites at different current densities.

are slightly shifted towards higher voltages (2.16, 1.28 and 0.80 eV) and the anodic peak potential is shifted to 2.50 eV. Fig. 4(b) shows the first three charge–discharge voltage profiles of the CuO/ MWCNT composites at the rate of 0.2 A·g^{-1}. It indicates that the first discharge curve exhibits a potential plateau at about 1.34 V. In the second discharge process, this potential plateau shifts upward close to 1.46 V and the curve becomes steeper. The initial discharge-charge capacities of the whole material of the CuO/MWCNT composites electrodes are 1555.6 mAh·g^{-1} and 699.3 mAh·g^{-1}, respectively. The initial coulombic efficiency of CuO/MWCNT is 44.9%. The main reason of the low coulombic efficiency at 1 cycle is the side reaction in the battery: the formation of a solid–electrolyte interphase (SEI) layer and the formation
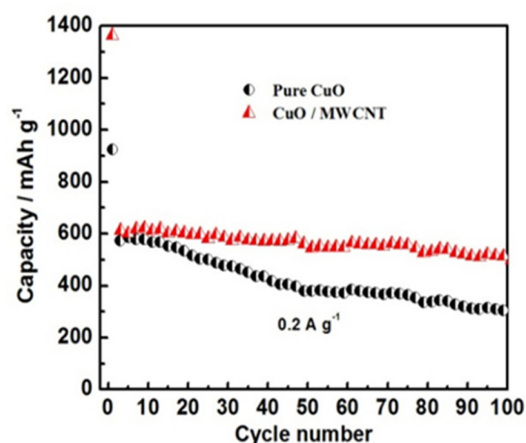
Fig. 6. Cycling performances of pure CuO and CuO/MWCNT composites at the current densities of 0.2 A·g^{-1}.
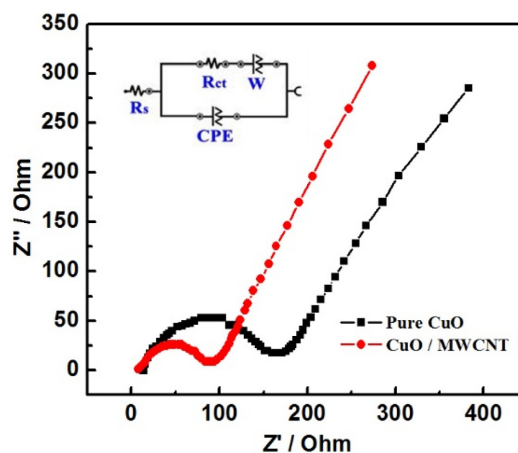

Fig. 7. Nyquist plots of pure CuO and CuO/MWCNT composites. Inset is the equivalent circuits.

Table 1. The performance of oxide anode material.

The active material	Initial coulombic efficiency	Initial discharge capacity (RT)	Capacity retention ratio (RT)	References
SnOx (hollow/amorphous)	51%	657.2 mAh·g^{-1}	81.3% (400 cycles, 500 mA·g^{-1})	[27]
Si@SiOx/C (Gyroid 3D Network)	80.1%	1635 mAh·g^{-1}	83.3% (100 cycles, 4000 mA·g^{-1})	[30]
Hollow CuO@C	48%	660 mAh·g^{-1}	92.4% (200 cycles, 100 mA·g^{-1})	[31]
nanosheets CuO/MWCNT	59.1%	686.9 mAh·g^{-1}	78.6% (50 cycles, 100 mA·g^{-1})	[28]
CuO hollow nanostructures	63.5%	614 mAh·g^{-1}	91.4% (50 cycles, 150 mA·g^{-1})	[32]
Hollow CuO/MWCNT (this work)	44.9%	699.4 mAh·g^{-1}	80% (100 cycles, 200 mA·g^{-1})	

of partial irreversible Li$_2$O originated from the surface oxide layers [27].

Rate cyclability of pure CuO and CuO/MWCNT composites are shown in Fig. 5. The CuO/MWCNT composites can still maintain the discharge capacities of 641.2, 568.7, 492.2 and 392.8 mAh·g^{-1} after 10 cycles at the current density of 0.2, 0.5, 1 and 2 A·g^{-1}, respectively. As a contrast, the rate capacities of pure CuO are 414.5, 138.2, 50.9 and 18.2 mAh·g^{-1} after 10 cycles at the current density of 0.2, 0.5, 1 and 2 A·g^{-1}, respectively. It is obvious that the CuO/MWCNT composites have an excellent rate capacity. Besides, the capacity of CuO/MWCNT composites recovered to 550.0 mAh·g^{-1} at a current density of 0.2 A·g^{-1} after

different rate cycles, better than that of the pure CuO whose capacity recovered to 167.3 mAh·g^{-1}. The cycling performances of pure CuO and CuO/MWCNT composites are shown in Fig. 6. It is clear that, compared to the pure CuO, the CuO/MWCNT composites have a better cycling performance. The initial capacity of the pure CuO and CuO/MWCNT are 572.8 mAh·g^{-1} and 612.3 mAh·g^{-1}, respectively. The pure CuO lost nearly half of capacity after 100 cycles at a current density of 0.2 A·g^{-1}. By contrast, the CuO/MWCNT composites have an excellent reversible capacity of 488.2 mAh·g^{-1} with a capacity retention ratio of 80%, after 100 cycles at a current density of 0.2 A·g^{-1}. Comparing to the nanosheets

CuO/MWCNT in reference 28 (78.6% capacity retention after 50 cycles), the CuO with a hollow structure has a better cycle performance. The detail performance information of oxide anode material are shown in Table 1. According to the Table 1, although the poor initial columbic efficiency is a negative factor of hollow structure oxide materials, they still have a substantial discharge capacity. Moreover, the hollow structure can obviously improve the stability of CuO/MWCNT electrode, which is also very important to the commercial production.

The better rate cyclability and cycling performance are attributed to the better electrical conductivity of MWCNTs, the hollow structure of CuO particles, and the flexible structure of the CuO/MWCNT composites. Through combining with MWCNTs, the better electrical conductivity is beneficial to reduce the resistance of the electrode. Fig. 7 is the Nyquist plots of pure CuO and CuO/MWCNT composites analyzed by EIS test. It is observed that the battery with the CuO/MWCNT anode has a much smaller AC impedance than that with the pure CuO anode. The smaller impedance improves the rate cyclability of the anode. Furthermore, the hollow structure of CuO particles and the flexible structure of the CuO/MWCNT composites reserves the space for the excessive volume change between the charge and discharge processes [29]. Thus, these special structures could relax the volume expansion, and slow the phenomenon of electrode pulverization and the collapse of the electrode, and then improve the cycling performance of the CuO/MWCNT composites.

4. Conclusions

The hollow CuO particles and MWCNT composites have been successfully synthesized through an optimized infiltration-reduction-oxidation method. The CuO/MWCNT composites have excellent rate ability capacities and cycle performances. The CuO/MWCNT composites have reversible capacity of 488.2 mAh·g^{-1} after 100 cycles at a current density of 0.2 A·g^{-1}. This improved synthetic method of the CuO/MWCNT composites is more facile and easy to control, which is more suitable for commercial production.

Acknowledgment

References

[1] M. Li, J. Lu, Z. Chen, and K. Amine, *Adv. Mat.*, **2018**, *30 (33)*, 1800561.

[2] G. Zubi, R. Dufo-López, M. Carvalho, and G. Pasaoglu, *Renewable and Sustainable Energy Rev.*, **2018**, *89*, 292-308.

[3] A. Re. Kamali, and D. J Fray, *J. New Mat. for Electrochem. Systems*, **2010**, *13(2)*, 147-160.

[4] B. Moradi, and G. G Botte, *J. Appl. Electrochem.*, **2016**, *46(2)*, 123-148.

[5] J. Wu, H. Chen, I. Byrd, S. Lovelace, and C. Jin, *ACS Appl. Mat. & Interfaces*, **2016**, *8(22)*, 13946-13956.

[6] Q. Xiong, H. Chi, J. Zhang and J. Tu, *J. Alloy Compd.*, **2016**, *688*, 729-735.

[7] H. Kim, W. Choi, J. Yoon, J. H. Um, W. Lee, J. Kim, J. Cabana, and W. Yoon, *Chem. Rev.,* **2020**.

[8] X. Li, A. Dhanabalan, and C. Wang, *J. Power Sources*, **2011**, *196(22)*, 9625-9630.

[9] C. Hou, S. Brahma, S. Weng, C. Chang, and J. Huang, *J. Electrochem. En. Conv. Stor.* **2020**, *17(3)*, 031003.

[10] W. Zhang, L. Feng, H. Chen, and Y. Zhang, *Nano*, **2019**, *14(09)*, 1950109.

[11] S. Ko, J. Lee, H. S. Yang, S. Park, and U. Jeong, *Adv. Mat.*, **2012**, *24(32)*, 4451-4456.

[12] M. Suleiman, M. Mousa, A. Hussein, B. Hammouti, T. B Hadda, and I. Warad, *J. Mat. and Environ. Sci.*, **2013**, *4(5)*, 792-797.

[13] X. Gao, J. Bao, G. Pan, H. Zhu, P. Huang, F. Wu, and D. Song, *J. Physical Chem. B*, **2004**, *108(18)*, 5547-5551.

[14] B. Wang, X. Wu, C. Shu, Y. Guo, and C. Wang, *J. Mat. Chem.*, **2010**, *20(47)*, 10661-10664.

[15] Z. Yin, Y. Ding, Q. Zheng, and L. Guan, *Electrochem. Commun.*, **2012**, *20*, 40-43.

[16] C. Wang, D. Higgins, F. Wang, D. Li, R. Liu, G. Xia, N. Li, Q. Li, H. Xu, and G. Wu, *Nano Energy*, **2014**, *9*, 334-344.

[17] A. Banerjee, U. Singh, V. Aravindan, M. Srinivasan, and S. Ogale, *Nano Energy*, **2013**, *2(6)*, 1158-1163.

[18] S. Wang, J. Zhang, and C. Chen, *Scripta Materialia*, **2007**, *57(4)*, 337-340.

[19] S. Xiao, D. Pan, L. Wang, Z. Zhang, Z. Lyu, W. Dong, X. Chen, D. Zhang, W. Chen, and H. Li, *Nanoscale*, **2016**, *8(46)*, 19343-19351.

[20] F. Pu, C. Kong, J. Lv, W. Zhang, X. Zhang, S. Yang, H. Jin, and Z. Yang, *J. Alloys and Compounds*, **2019**, *805*, 355-362.

[21] S. Jia, Y. Wang, X. Liu, S. Zhao, W. Zhao, Y. Huang, Z. Li, and Z. Lin, *Nano Energy*, **2019**, *59*, 229-236.

[22] X. Chen, C. Yu, X. Guo, Q. Bi, M. Sajjad, Y. Ren, X.

Zhou, and Z. Liu, *Nano*, **2018**, *13(09)*, 1850103.

[23] Z. Zhu, L. R Radovic, and G. Lu, *Carbon*, **2000**, *38(3)*, 451-464.

[24] Y. Yin, R. M Rioux, C. K Erdonmez, S. Hughes, G. A Somorjai, and A P. Alivisatos, *Science,* **2004**, *304(5671)*, 711-714.

[25] A. Debart, L. Dupont, P. Poizot, J. Leriche, and J. Tarascon, *J. Electrochem. Soc.*, **2001**, *148(11)*, A1266.

[26] H. Yin, X. Yu, Q. Li, M. Cao, W. Zhang, H. Zhao, and M. Zhu, *J. Alloys and Compounds*, **2017**, *706*, 97-102.

[27] X. Zhao, W. Wang, Z. Hou, Y. Yu, Q. Di, X. Wu, G. Wei, Z. Quan, and J. Zhang, *Inorganic Chemistry Frontiers*, **2019**, *6(2)*, 473-476.

[28] W. Yuan, Z. Qiu, Y. Chen, B. Zhao, M. Liu, and Y. Tang, *Electrochim. Acta,* **2018**, *267*, 150-160.

[29] J. Xiang, J. Tu, J. Zhang, J. Zhong, D. Zhang, and J. Cheng, *Electrochem. Commun.*, **2010**, *12(8)*, 1103-1107.

[30] J. Lee, J. Moon, S. A Han, J. Kim, V. Malgras, Y.-U. Heo, H. Kim, S.-M. Lee, H. K. Liu, and S. X. Dou, *ACS nano*, **2019**, *13(8),* 9607-9619.

[31] Y. Dong, X. Jiang, J. Mo, Y. Zhou, and J. Zhou, *Chem. Eng. J.*, **2020**, 381, 122614.

[32] J. C. Park, J. Kim, H. Kwon, and H. Song, *Adv. Mat.*, **2009**, *21(7)*, 803-807.